

Hierarchical Cluster Analysis to Aid Diagnostic Image Data Visualization of MS and Other Medical Imaging Modalities

SELVAN, Arul, COLE, Laura, SPACKMAN, Lynne and WRIGHT, Chris

Available from Sheffield Hallam University Research Archive (SHURA) at:

<http://shura.shu.ac.uk/15710/>

This document is the author deposited version. You are advised to consult the publisher's version if you wish to cite from it.

Published version

SELVAN, Arul, COLE, Laura, SPACKMAN, Lynne and WRIGHT, Chris (2017). Hierarchical Cluster Analysis to Aid Diagnostic Image Data Visualization of MS and Other Medical Imaging Modalities. In: COLE, Laura, (ed.) Imaging Mass Spectrometry Methods and Protocols. Methods in Molecular Biology, 1 . Humana Press, 95-123.

Repository use policy

Copyright © and Moral Rights for the papers on this site are retained by the individual authors and/or other copyright owners. Users may download and/or print one copy of any article(s) in SHURA to facilitate their private study or for non-commercial research. You may not engage in further distribution of the material or use it for any profit-making activities or any commercial gain.

Chapter 10

Hierarchical Cluster Analysis to Aid Diagnostic Image Data Visualization of MS and Other Medical Imaging Modalities

Arul N. Selvan, Laura M. Cole, Lynne Spackman, Sarah Naylor, and Chris Wright

Abstract

Perceiving abnormal regions in the images of different medical modalities plays a crucial role in diagnosis and subsequent treatment planning. In medical images to visually perceive abnormalities' extent and boundaries requires substantial experience. Consequently, manually drawn region of interest (ROI) to outline boundaries of abnormalities suffers from limitations of human perception leading to inter-observer variability. As an alternative to human drawn ROI, it is proposed the use of a computer-based segmentation algorithm to segment digital medical image data.

Hierarchical Clustering-based Segmentation (HCS) process is a generic unsupervised segmentation process that can be used to segment dissimilar regions in digital images. HCS process generates a hierarchy of segmented images by partitioning an image into its constituent regions at hierarchical levels of allowable dissimilarity between its different regions. The hierarchy represents the continuous merging of similar, spatially adjacent, and/or disjoint regions as the allowable threshold value of dissimilarity between regions, for merging, is gradually increased.

This chapter discusses in detail first the implementation of the HCS process, second the implementation details of how the HCS process is used for the presentation of multi-modal imaging data (MALDI and MRI) of a biological sample, third the implementation details of how the process is used as a perception aid for X-ray mammogram readers, and finally the implementation details of how it is used as an interpretation aid for the interpretation of Multi-parametric Magnetic Resonance Imaging (mpMRI) of the Prostate.

Key words Image perception, Image processing, Segmentation, Computer-aided detection, Computer-aided diagnosis, MALDI, MSI, MRI, Mammogram, DCE-MRI, mpMRI

1 Introduction

Tissue abnormality in medical images is usually related to a dissimilar part of an otherwise homogeneous image. The dissimilarity may be subtle or strong depending on the medical modality and the type of abnormal tissue.

Segmentation and delineation of abnormalities in medical images plays an important role in diagnosis and subsequent treatment planning. For example when an abnormality is identified by

a radiologist on a breast screening mammogram then this case is discussed in detail at a multidisciplinary team (MDT) meeting to determine appropriate follow-up. It is important that the lesion extent is appropriately understood and delineated at the MDT in the communication between radiologist and surgeon concerning such abnormal cases which requires some form of region excised. It is well known that disagreements exist concerning the definition of lesion extent and the accurate specification of the location of lesion edges. This issue is important because of the following:

- The potential extent of treated abnormal area can determine what type of subsequent surgical intervention the woman has and
- Surgeons typically excise more breast material surrounding a lesion to ensure that they have fully removed any malignancy.

To visually perceive abnormalities' extent and boundaries requires substantial experience. Consequently, manually drawn region of interest (ROI) to outline boundaries of abnormalities suffers from the following limitations:

- Abnormalities are heterogeneous, hence in manually drawn region of interest (ROI) due to the limitation of human perception information on abnormalities' heterogeneity remains poorly exploited.
- Also manual ROI suffers from inter-observer variability.

As an alternative (to ROI based), it is proposed the use of a segmentation algorithm, for example by Chandarana et al. [1]. In medical images, segmentation of regions of potential abnormalities is a difficult task because of issues such as spatial resolution, poor contrast, ill-defined boundaries, noise, or acquisition artifacts [2].

Segmentation can be thought as a process of grouping visual information, where the details are grouped into objects, objects into classes of objects, etc. Thus, starting from the composite segmentation, the perceptual organization of the image can be represented by a tree of regions, ordered by inclusion. The root of the tree is the entire scene, the leaves are the finest details, and each region represents an object at a certain scale of observation [3].

Traditionally, segmentation algorithms would "binarize" the boundary map by choosing some threshold. There are two problems with thresholding a boundary map [4]:

- The optimal threshold depends on the application, and
- Thresholding a low-level feature like boundaries is likely to be a bad idea for most applications, since it destroys much information.

For these reasons, the segmentation algorithm should operate on a non-thresholded basis. Nevertheless, one needs to threshold the boundary map in order to perceive the boundaries, but this is done at many levels.

Hierarchical Clustering-based Segmentation (HCS) process is an unsupervised segmentation process that generates a hierarchy of segmented images by partitioning an image into its constituent regions at hierarchical levels of allowable dissimilarity between its different regions. The hierarchy represents the continuous merging of similar, spatially adjacent, and/or disjoint regions as the allowable threshold value of dissimilarity between regions, for merging, is gradually increased [5–7].

This chapter discusses in detail the implementation of the HCS process and how the process is applied for the following:

- HCS aided presentation of multi-modal (Magnetic Resonance Imaging—MRI and Matrix-Assisted Laser Desorption/Ionization—MALDI, Mass Spectrometry Imaging—MSI) imaging data of biological tissue sample.
- HCS as a perception aid for X-ray mammogram readers.
- HCS aided interpretation of Multi-parametric Magnetic Resonance Imaging (mpMRI).

2 Materials

The input to the HCS process is a two-dimensional matrix of numbers. The two-dimensional matrix of numbers can be the representation of the distribution of masses (of peptide and protein) in a biological sample (in the case of MALDI MSI) or the attenuated X-ray energy (in the case of X-ray images) or the nuclear magnetic resonance signal from the hydrogen atoms in an object (in the case of MRI). In the following three sections, the acquisition details of the input data, for each of the three applications of the HCS process, is discussed separately.

2.1 MRI and MALDI-MSI Data of Tissue Sample

The tissue sample was subcutaneously transplanted mouse fibrosarcoma tumors. The MRI sectional images and subsequently MALDI MSI data were acquired as follows [8]:

- The tumor tissue was embedded in gelatin blocks and markers were placed in all four corners of the gelatine blocks in order to aid spatial recognition and registration between modalities (Fig. 1).
- MRI images were acquired using the 0.25 T Esaote GScan. The sample was centrally placed with a dedicated wrist coil and a range of sequences performed FOV (160 × 160). Optimal results were achieved from the T2-weighted Gradient Echo (3NEX) and XBone (4NEX) sequences; 2 mm slices (*see* **Notes 1 and 2**) (Fig. 2).

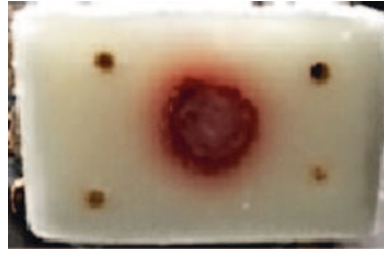


Fig. 1 Tumor tissue embedded in a gelatin block and four markers placed in four corners

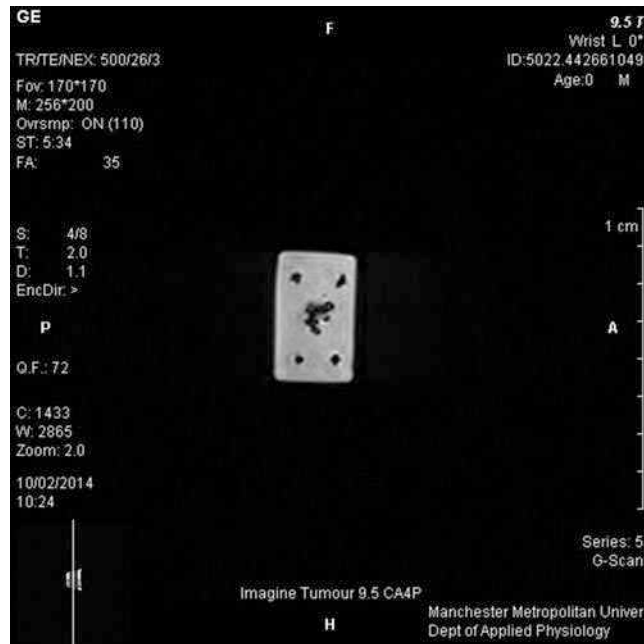


Fig. 2 T2-weighted MRI image of the tissue specimen

- The tissue sample was frozen and then cryosectioned prior to MALDI MSI data capture.
- Peptide mass fingerprints and MALDI Images were performed using the Applied Biosystems Qstar Pulsar i.

2.2 X-Ray Mammogram Image Data

Anonymized X-ray mammogram image data were acquired as part of a screening program using Full Field Digital Mammography (FFDM) system with the pixel spacing of $70 \mu\text{m}$ (0.070 mm) (*see Note 3*). The approximate location and extent of abnormalities were marked by an expert radiologist (Fig. 3).

2.3 mpMRI Image Data

Anonymized MRI image data were acquired as part of diagnostic investigation. The images were acquired with pixel spacing of $1000 \mu\text{m}$ (1.0 mm) and 1.0 mm spacing between slices. The multi-parametric

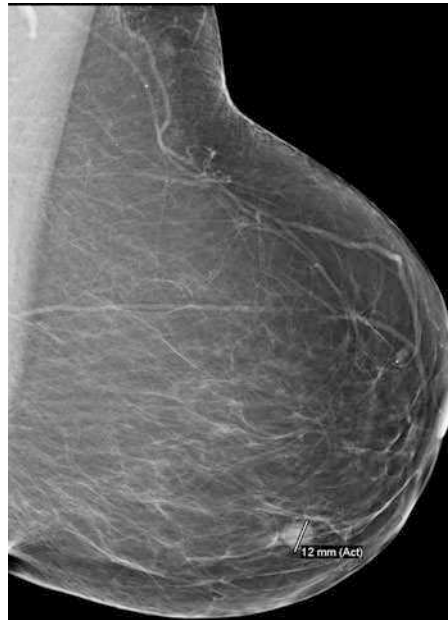


Fig. 3 X-ray mammogram image with the location and size of the abnormality marked by the expert

images were acquired as T2-weighted before injecting intravenous contrast (Fig. 4) and T1-weighted Dynamic Contrast Enhanced (DCE) images. In T2-weighted images, with a small "Field Of View" (FOV), tumour will appear as signal loss (dark).

The DCE MRI images are acquired after intravenously injecting gadolinium chelate contrast (Fig. 5). After injecting intravenous contrast the temporal sections were acquired 16 times at an interval of approximately 10.49 s. Figure 6 lists the Prostate part of the section acquired from time 10:23:51.6275 (SER26) to time 10:26:33.9775 (SER11) (Fig. 6).

3 Methods

In the interpretation of medical images visually perceiving the different component regions in the image is a difficult task, this is due to issues like spatial resolution, poor contrast, ill-defined boundaries, noise, or acquisition artifacts [2]. To aid the visual perception and thus facilitate the interpretation process, the HCS process was adopted to outline and highlight the different regions in an image.

In the following sections, first the HCS process method is outlined. In subsequent sections, it will be discussed in detail how the HCS process was used for the following:

- To visualize the correlating information between the two modalities MRI and MALDI-MSI.



Fig. 4 T2-weighted MRI image section of the prostate

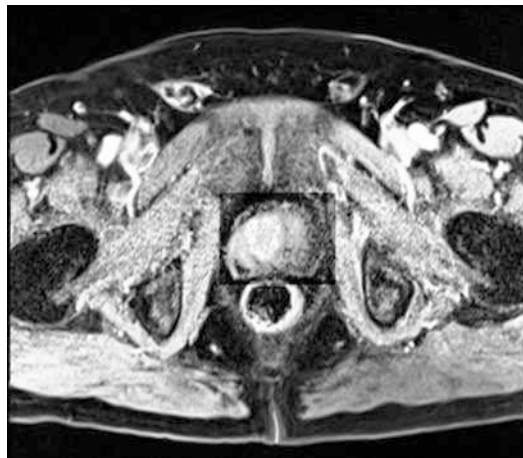


Fig. 5 Dynamic Contrast Enhanced MRI image section of the Prostate post contrast injection

- To visualize the finer details within a potential abnormal region in a X-ray mammogram.
- To visualize multi-parametric MRI image data (T1-weighted DCE-MRI and T2-weighted MRI) and thus correlate information between the two parametric image data.

3.1 Hierarchical Clustering-Based Segmentation (HCS)

Since the early days of computer vision, the hierarchical structure of visual perception has motivated clustering techniques to segmentation [9], where connected regions of the image domain are classified according to an inter-region dissimilarity measure. Hierarchical Clustering-based Segmentation (HCS) [5–7] implements the traditional agglomerative clustering [10], where the regions of an initial partition are iteratively merged and automatically generate a hierarchy of segmented images. The hierarchy of

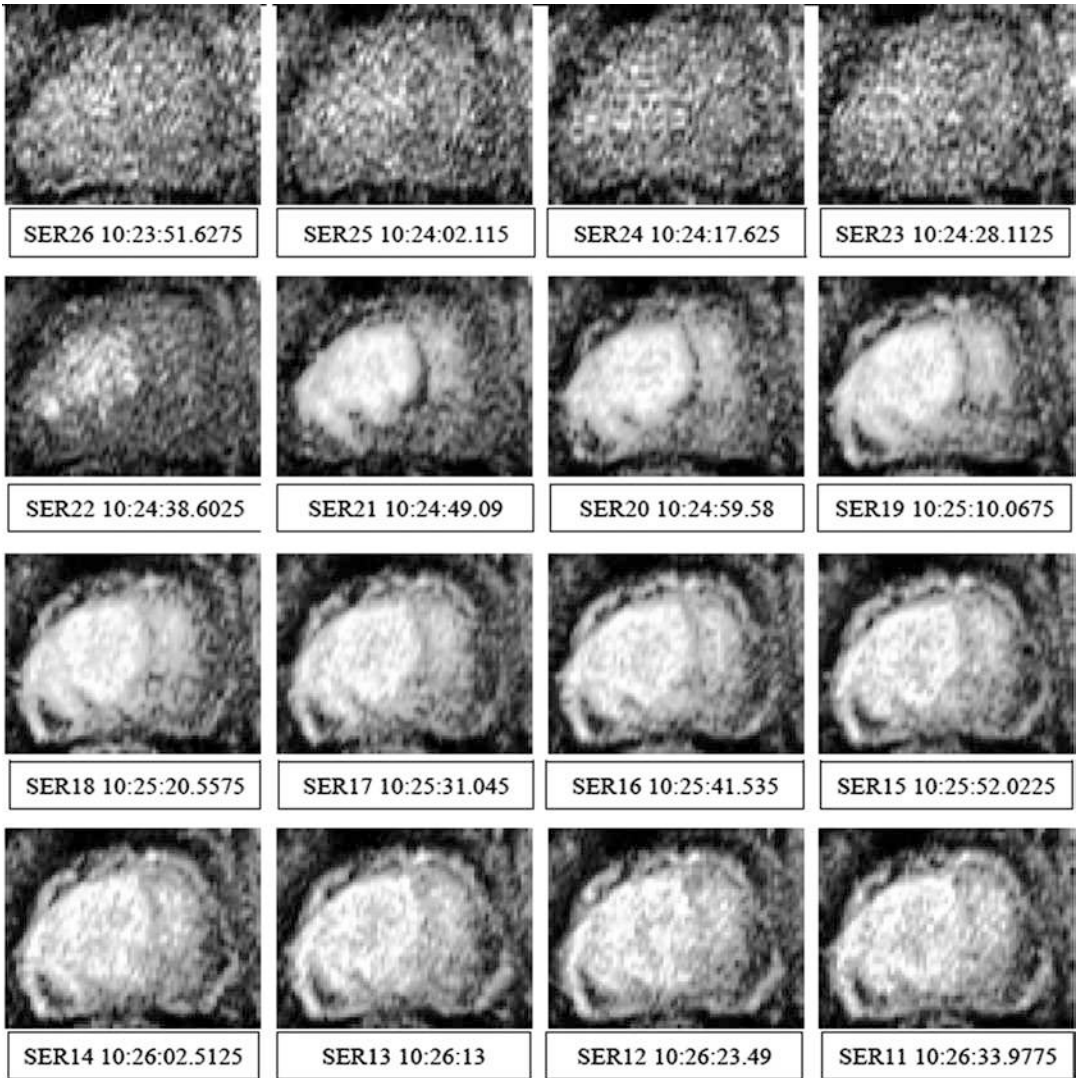


Fig. 6 Temporal sequence of the DCE MRI image of a section of the Prostate

segmented images is generated by partitioning an image into its constituent regions at hierarchical levels of allowable dissimilarity between its different regions. At any particular level in the hierarchy, the segmentation process will cluster together all the pixels and/or regions that have dissimilarity among them less than or equal to the dissimilarity allowed for that level. Refer Fig. 7 for a flowchart representation of the HCS process.

Following is a high-level description of the HCS process (Fig. 7) [5]:

1. Give each pixel in the image a region label as follows:
 - If an initial segmentation of the image is available, label each pixel according to this pre-segmentation.

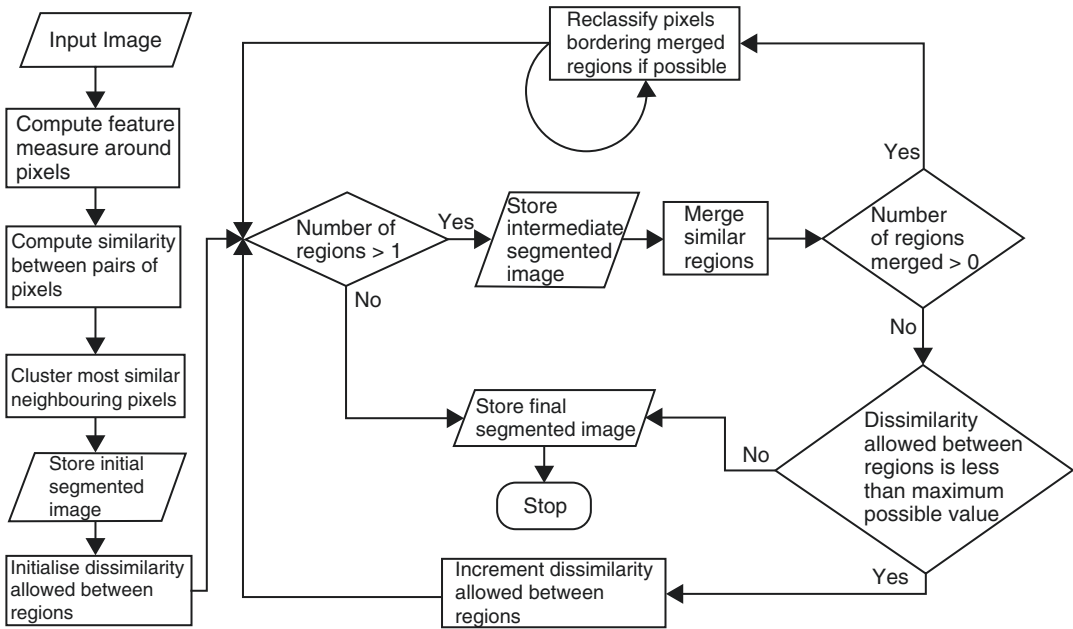


Fig. 7 Flowchart illustrating the HCS process' operational logic

If no initial segmentation is available, label each pixel as a separate region.

Set current dissimilarity allowed between regions, *dissimilarity_allowed*, equal to zero.

2. Calculate the dissimilarity value, (*dissimilarity_value*), between all pairs of regions in the image.

Set *threshold_value* equal to the smallest *dissimilarity_value*.

3. If the *threshold_value* found, in **step 2**, is less than or equal to the current *dissimilarity_allowed*, then merge all those regions having *dissimilarity_value*, between them, less than, or equal to the *threshold_value*. Otherwise go to **step 6**.

4. If the number of regions merged in **step 3** is greater than 0, then reclassify the pixels on the border of the merged regions with the rest of the regions until no more reclassification is possible.

After all the possible border pixels are reclassified, among the merged regions, store the region information for this iteration as an intermediate segmentation and go to **step 2**.

Otherwise, if the number of regions merged in **step 3** is equal to 0 then, go to **step 5**.

5. If the current number of regions in the image is less than the preset value, *check_no_regions*, go to **step 7**.
Otherwise, go to **step 6**.
6. If the current value of *dissimilarity_allowed* is less than the maximum possible value, then increase the *dissimilarity_allowed* value by an incremental value, and go to **step 2**.
Otherwise go to **step 7**.
7. Save the region information from the current iteration as the coarsest instance.

The above steps are processing intensive but ensure that the segmentation does not depend on the order in which the image regions are processed and the borders identified are more appropriate (*see* **Notes 4** and **5**).

3.2 HCS Process Aided Correlation of MRI and MALDI-MSI Image Data

The details of the steps followed in preparing the tissue sample and acquiring the corresponding MALDI-MSI data for this study is given in another publication [11] coauthored by the author. Following are the steps involved in correlating the MRI image data of the tissue with that of the MALDI-MSI data (Figs. 8 and 9).

- The original MRI image data was up-sampled (*see* **Notes 1** and **2**).
- The HCS process was applied within the region of interest (ROI) enclosing the tissue.
- The typical segmentation output was identified.
- The HCS segmentation output was correlated (visually) with the MALDI-MSI (Fig. 9).

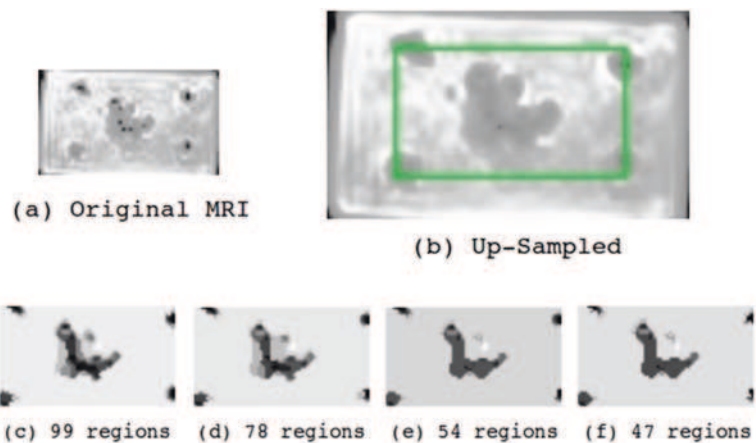


Fig. 8 Processing of the T2-weighted MRI image section (a) of the tissue specimen. The original image data is Up-Sampled (b). The HCS process relevant output highlighting the inner details of the abnormality (c, d)

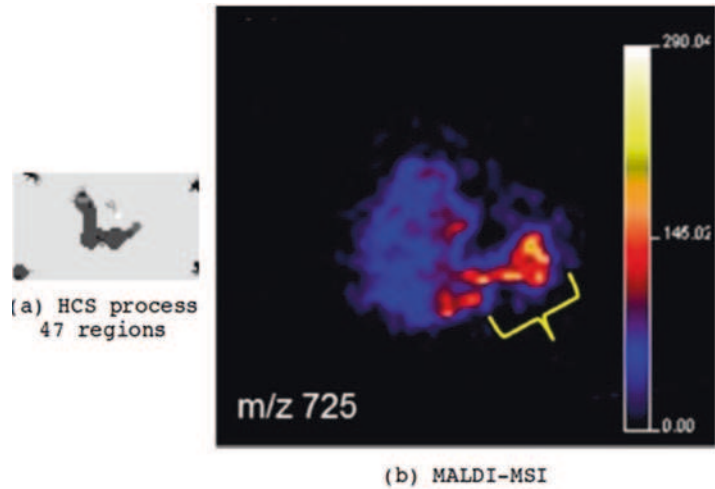


Fig. 9 Correlation of the HCS process' highlighted inner details of the abnormality with the MALDI-MS image

The primary requirement of an automated abnormalities detection system (like HCS) is the segmentation of the potential abnormal regions from noise and background. Segmentation of regions of abnormalities in images of low resolution is a challenging task. However, still, from the output in Figs. 8 and 9 one can infer that there is a potential for this approach (*see Note 6*).

3.3 HCS Process as a Perception Aid in Delineating Abnormalities in X-Ray Mammograms

Computer-aided detection (CAD) systems offer prompts to alert the reader to potential abnormalities. Hierarchical Clustering-based Segmentation (HCS) goes further by identifying the more appropriate edges of a lesion and heterogeneous regions within. The following method was adopted to evaluate how the HCS process outputs aid in the visualization of the details within the abnormalities in X-ray mammograms.

- Since the main aim is to aid the user to visualize the finer details of an abnormal region, to start with the approximate location and extent of the abnormality is marked by the user (Fig. 10).
- Since the original image data is of very high resolution and since the HCS process is processing intensive the original image data was subsampled (*see Notes 3 and 4*) (Fig. 11).
- The HCS process was applied to the subsampled image data within the ROI and for the HCS process's relevant segmentations following three types of output were created (*see Note 7*).

Boundary outlined dissimilar regions (Fig. 12).

Heat map of the dissimilar regions (Fig. 13).

Highlighted dissimilar regions (Fig. 14).

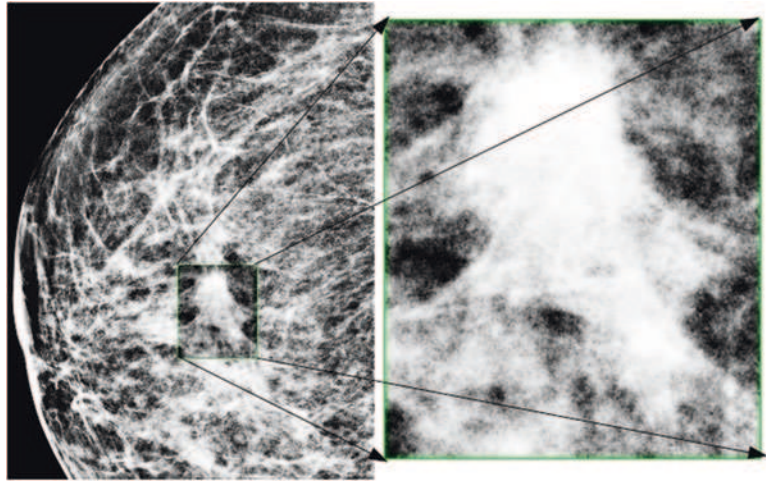


Fig. 10 Part of the original X-ray mammogram image with the part of the image having the abnormality enlarged

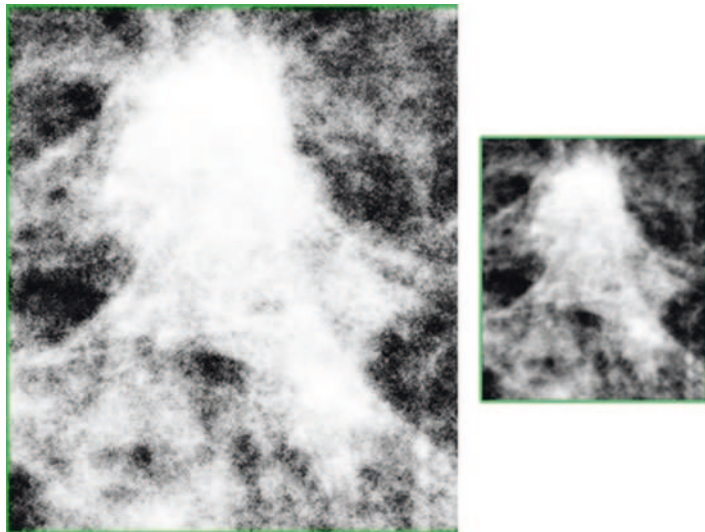


Fig. 11 Original size of the part of the image containing the abnormality and a reduced size of it after applying bilinear subsampling to the original data

We set out to determine whether the HCS process's output would be useful and offer a potential computer-based decision aid in that it can aid in the identifying of the appropriate edges of a lesion and heterogeneous regions within that lesion area.

An initial pilot study was conducted as an online study.

[https://shusls.qualtrics.com/SE/?SID=SV_20oJptApsrst2xT].

The study participants were asked a few standard demographic questions and a couple of questions regarding their current use of computer-aided detection when interpreting mammograms. In the

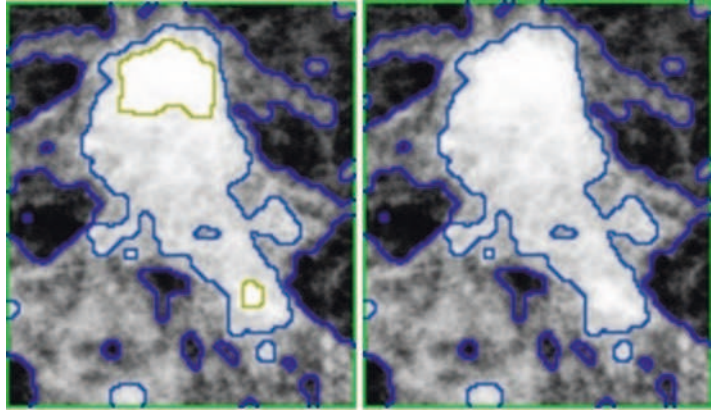


Fig. 12 HCS process' boundaries outlining the, hard to visualize, finer inner details of the abnormality

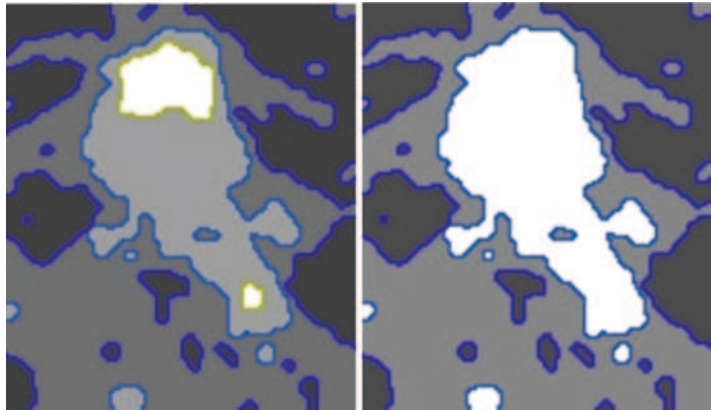


Fig. 13 Heat map image of the different dissimilar regions, within the abnormality, found by the HCS process

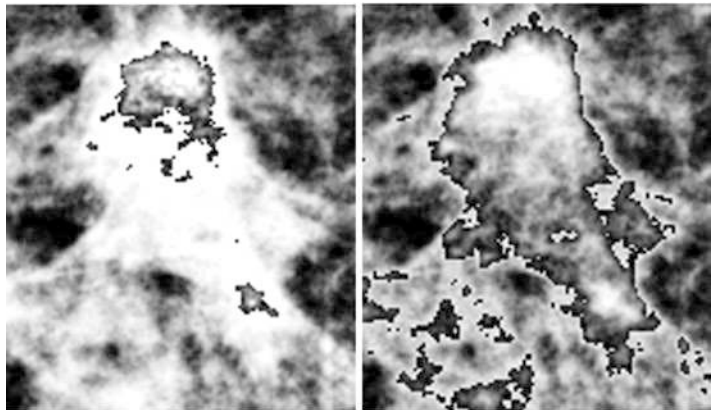


Fig. 14 Highlighted parts of the abnormality which are found to be dissimilar from the surrounding region

main task of the study the participants were presented with six mammograms, with a region of interest containing a suspected lesion already marked [12].

In condition 1, they were asked to examine this region and to indicate the extent of the lesion by using the mouse to place markers on the outer edges of the lesions. Participants were then asked whether or not they thought the lesion was multifocal and whether they thought it might be malignant.

In addition to the images shown on the screen, the original DICOM images were made available for them to download if they wish. After completing this they were then asked to repeat the task, but this time taking into consideration the additional information provided by the HCS process's output aids (condition 2) [12].

In the pilot study, the absolute differences in lesion measurements and the inter-subject reliability were compared between the two conditions. The intraclass correlation coefficient was used as an estimate of reliability and was similar between the two conditions (0.59, 0.57) [12].

When the images were divided into two groups, lesions with distinct borders and lesions with diffuse borders, there was a significant change in the absolute differences in the lesion measurements when the lesion borders were indistinct, but not in the images where the lesion borders were clearly defined.

Posthoc tests showed a significant difference in the lesion measurements when using the HCS output in cases when the lesion boundaries were indistinct ($t(2) = -7.42, p = 0.018$) than when the lesion boundaries were clearly defined ($t(2) = -1.54, p = 0.263$) [12].

HCS processing confirms the heterogeneous nature of seemingly homogeneous tissue. The adjustment of the lesion extent and increased confidence in making diagnostic interpretations by the mammogram reader in this study suggests that this information would be of practical use, particularly in cases where the lesion boundary information is ambiguous or indistinct (Fig. 15). This facilitates the accurate targeting of biopsy to the core of suspected

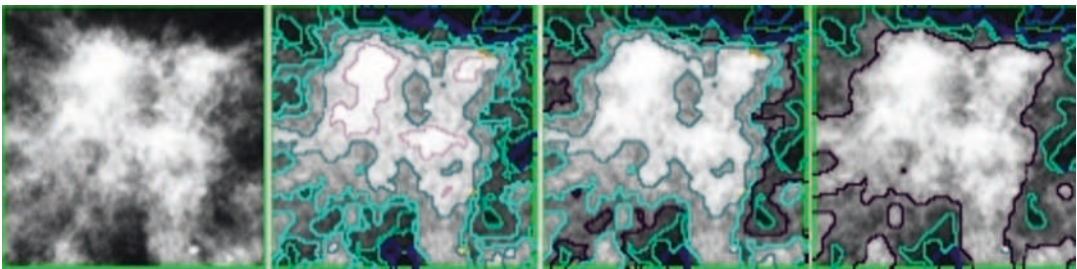


Fig. 15 Abnormality with regions having ill-defined boundaries and the HCS process' outlining of their boundaries

abnormality. Another key application is in the monitoring of tissue during and after treatment to assess the effect of drug and/or radiotherapy [12].

3.4 HCS Process Aided Interpretation of Multi-Parametric MRI (mpMRI) of Prostate

Studies have demonstrated that information from the T2-weighted MR images has a diagnostic performance such that it complements a DCE T1-weighted-based computer-aided diagnostic (CADx) system in discriminating malignant lesions from normal and benign regions [13].

Prostate Imaging and Reporting and Data System Version 2 (PI-RADS v2) recommends DCE should be included in all prostate mpMRI exams so as not to miss some small significant cancers. The DCE data should always be closely inspected for focal early enhancement. If found, then the corresponding T2 W and DWI images should be carefully interrogated for a corresponding abnormality.

From the above discussion, it can be inferred that mpMRI plays a key role in the detection of Prostate cancer. In this section, we will discuss how the HCS process aids in the interpretation of mpMRI of the Prostate.

Following are the steps that are involved in the HCS process-aided interpretation of mpMRI of the prostate:

- Time Intensity Curves (TIC)-based evaluation of DCE MRI Images.
- HCS process analysis of the corresponding T2-weighted MR image section.
- Correlating the HCS highlighted regions in the T2-weighted MRI image section, with the DCE-MRI TIC-based classification.

Each of the above steps will be discussed in detail below.

3.4.1 Time Intensity Curves (TIC)-Based Evaluation of DCE MRI Images

In prostate cancer, the leaky characteristics of the tumor angiogenesis are demonstrated in DCE-MRI by the early rapid high enhancement just after the administration of contrast medium followed immediately by a relatively rapid decline. In comparison there will be a slower and continuously increasing enhancement for normal tissues [14]. The visual analysis of DCE-MRI data makes use of the above phenomena. However, the visual assessment is inherently subjective.

The above characteristics can also be demonstrated by the quantitative measurement of signal enhancement in DCE- MRI with time. The characteristic shapes of the Time intensity curves (TIC) (Fig. 16) may be used for supporting diagnosis (*see Note 8*).

To categorize the TIC the shape of the TIC is analyzed as follows:

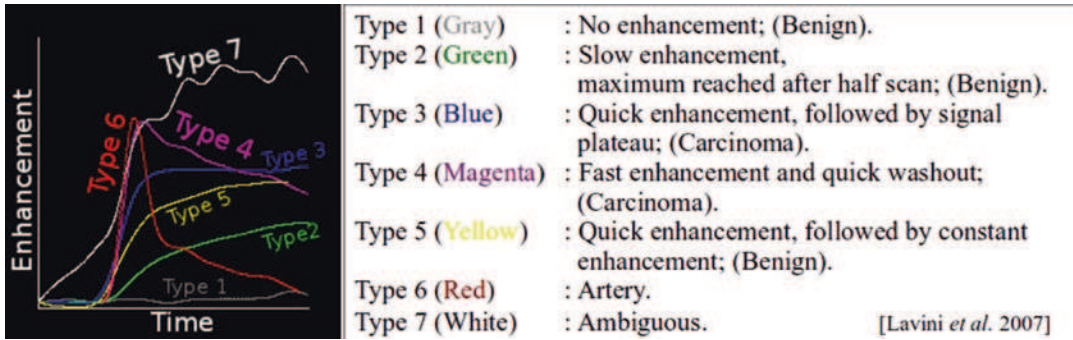


Fig. 16 Different shapes of the Time Intensity Curve (TIC) and their significance [15]

- The signal baseline (SB) was arbitrarily calculated as the average signal intensity of initial three time points before the positive slope occurs ($tp = 0$).
- The Tail of the TIC was assumed as the last three quarters of the time points after ($tp = 0$).
- The intercept (α) of the line fitted to the tail, with the axis crossing the time axis at the time $tp = 0$ and the tangent (β) of this line at the last time point was found.

To analyze the shape of the TIC the following features were used [15]

- ME: (MSD/SB) , where MSD (Maximum signal difference) is the difference between the signal intensity at its maximum $S(\max)$ and SB.
- TTP: Time difference (in seconds) between the moment where the ME occurs and at ($tp = 0$). For increase-only TICs, the TTP is the last time point in the scan.
- MSI: Largest positive signal difference between two successive scans.
- RelFS: β/MSD . To describe the behavior of the curves in the last part of the scan: whether it is flat (RelFS =0), declining (RelFS <0), or increasing (RelFS >0).

For the DCE-MRI of the prostate the different TIC types (Fig. 16) are classified by a decision tree based on the above features and their threshold values listed in Fig. 17.

The HCS process-based TIC shape analysis starts with the HCS process applied to the user-selected section within a ROI (Fig. 18). The HCS process output provides the heat map images based on the normalized average pixel value of the various dissimilar regions and the regions' boundaries (Fig. 19). TICs of the

TIC Type	ME	TTP	MSI	Re1FS
1	< ME threshold			
2	> ME threshold	> 1/2 tp(maximum)	< MSD/2.0	> 0.25
3	> ME threshold		> MSD/2.0	-0.25 < Re1FS < 0.25 (Flat Tail)
4	> ME threshold	< 1/2 tp(maximum)	> MSD/4.0	Re1FS < -0.25 (Declining Tail)
5	> ME threshold	> 1/2 tp(maximum)	> MSD/2.0	Re1FS > 0.25 (Positive slope Tail)

Fig. 17 The values of the TIC curve parameters to differentiate the TIC and categorize them [15]

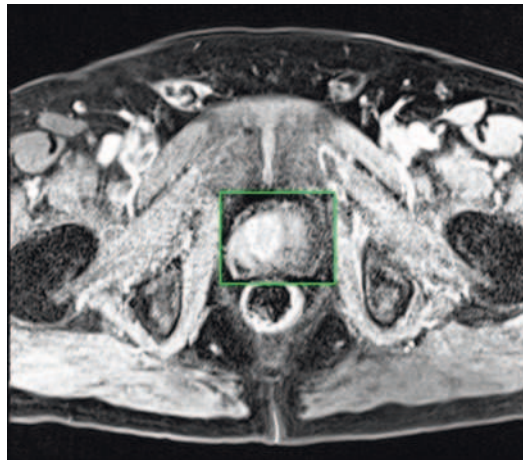


Fig. 18 DCE-MRI image section of the prostate with the region of interest (ROI) enclosing the Prostate marked. The HCS process will be applied within the ROI

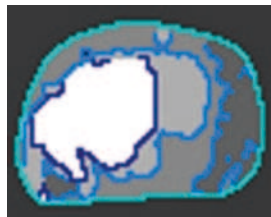


Fig. 19 Heat map image to show the different regions identified by the HCS process. The regions are shaded (*bright to dark*) based on the average pixel value of the region. The boundaries are marked by *random unique color*

contrast wash-in, wash-out process are then plotted for suspicious regions confirmed by the user (Figs. 20, 21, and 22). All the regions in the image are classified and colored based on the type of TIC for that region (Fig. 23).

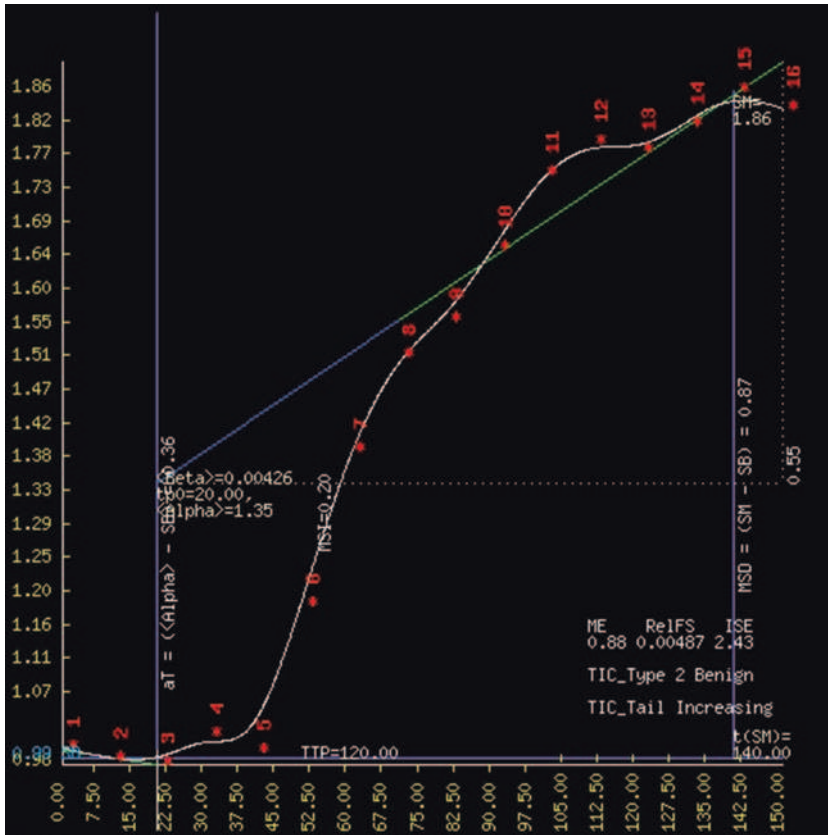


Fig. 20 Parametric illustration of the TIC of the part of the organ which is healthy. The program has automatically categorized the TIC, based on the curve’s parameters, as Type 2 (Benign)

3.4.2 HCS Process Analysis of the Corresponding T2-Weighted MR Image Section

The corresponding T2-weighted MRI image section is identified. This can be done making use of the DICOM viewer and viewing the DCE-MRI image sections and the T2-weighted image sections side by side (Fig. 24). The HCS process is applied to the identified T2-weighted image section (Fig. 25) to process only the Prostate part of the section (Fig. 26).

From the HCS process output the relevant segmentation’s region image (Fig. 27) and the boundary image (Fig. 28) are identified.

3.4.3 Correlating the HCS Highlighted Regions in the T2-Weighted MRI Image Section, with the DCE-MRI TIC-Based Classification

The HCS process’s segmentation output of the T2-weighted image has outlined an area of signal loss (dark) (Fig. 28). Tumor in T2-weighted will appear as signal loss. But false positives occur in hemorrhage, calcification, inflammation, and fibrosis [post-inflammatory, postoperative, posthormonal (ADT), post-radiation, or following thermal ablation treatment].

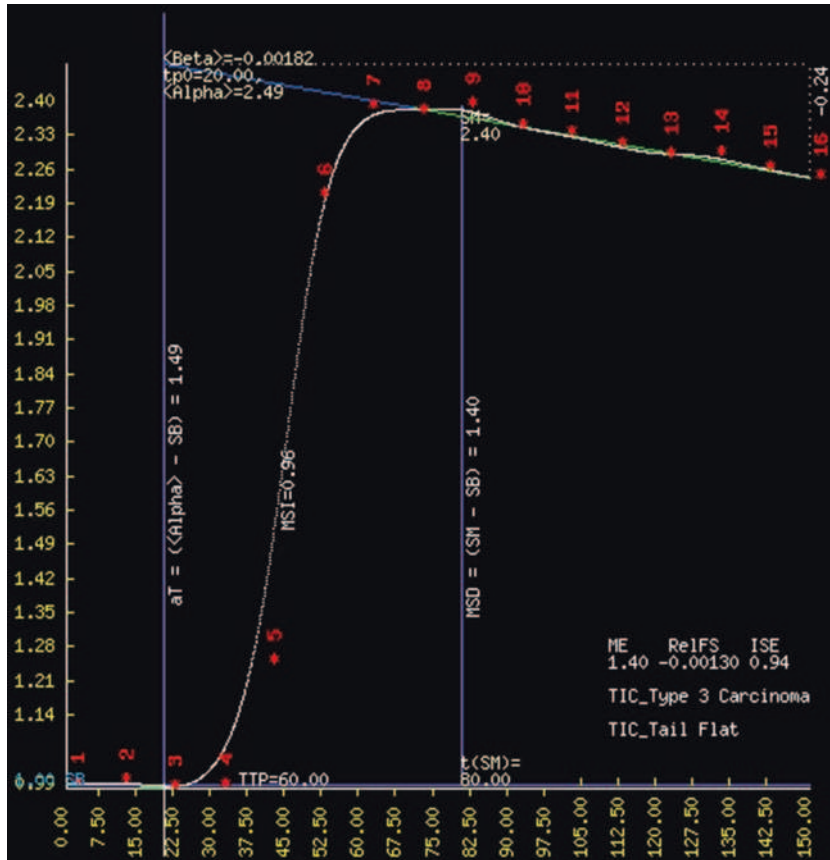


Fig. 21 Parametric illustration of the TIC of the part of the organ which has got a malignancy. The program has automatically categorized the TIC, based on the curve's parameters, as Type 3 (carcinoma)

So to confirm whether the signal loss in the T2-weighted image is due to tumor, the DCE-MRI TIC-based classification is made use of. In this case, the corresponding region, where there is signal loss in the T2-weighted image, is classified as Type-3 carcinoma (Blue) (Fig. 23).

Thus by correlating HCS boundary outlined T2-weighted image with the DCE-MRI TIC-based classified regions (Fig. 29), it can be confirmed that the signal loss in T2-weighted image is indeed due to tumor.

To ease the viewing of the different HCS segmentation output interactively and view both the T2-weighted image and the DCE-MRI image side by a GUI like the one shown in Fig. 30 can be used (Fig. 30).

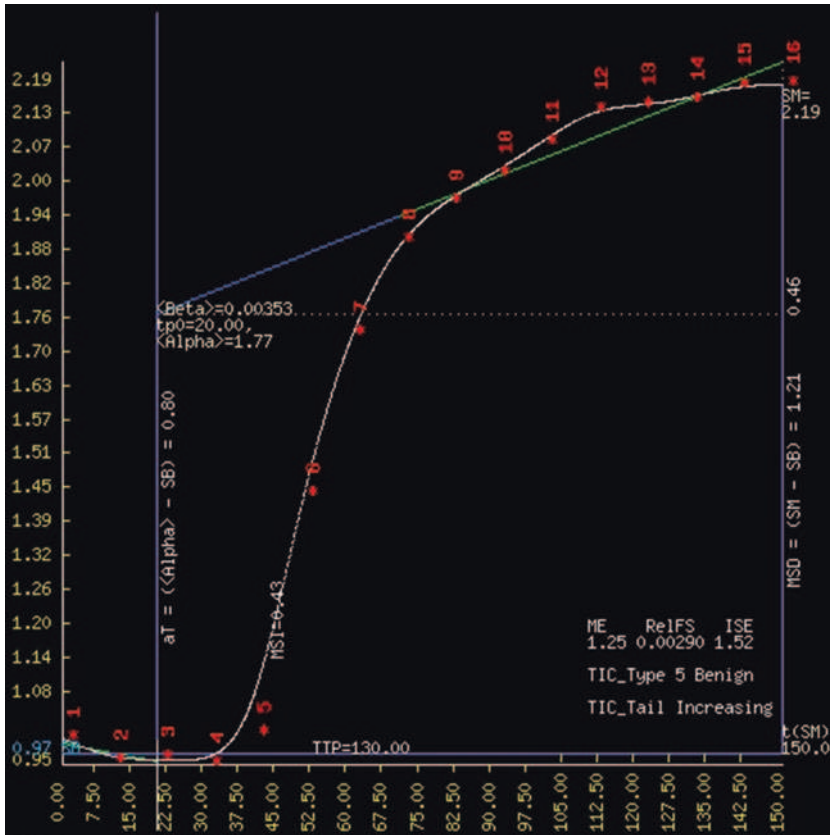


Fig. 22 Parametric illustration of the TIC of the part of the organ which is healthy. The program has automatically categorized the TIC, based on the curve's parameters, as Type 5 (Benign)



Fig. 23 The HCS process identified regions categorized as tumor (*Blue*) or healthy (*Yellow, Green*) based on the enhancement pattern (TIC shape) of the pixels within the region. The color coding is based on the six different types of enhancement patterns (Fig. 16)

4 Notes

1. The images were acquired by an MR equipment (with permanent magnet) having a magnetic field strength of 0.25 T and the pixel resolution was 500- μm (0.5-mm). In comparison diagnostic MRI equipment (equipped with super-conductive magnets) normally has a magnetic field strength ranging from 1.5 to 3 T.

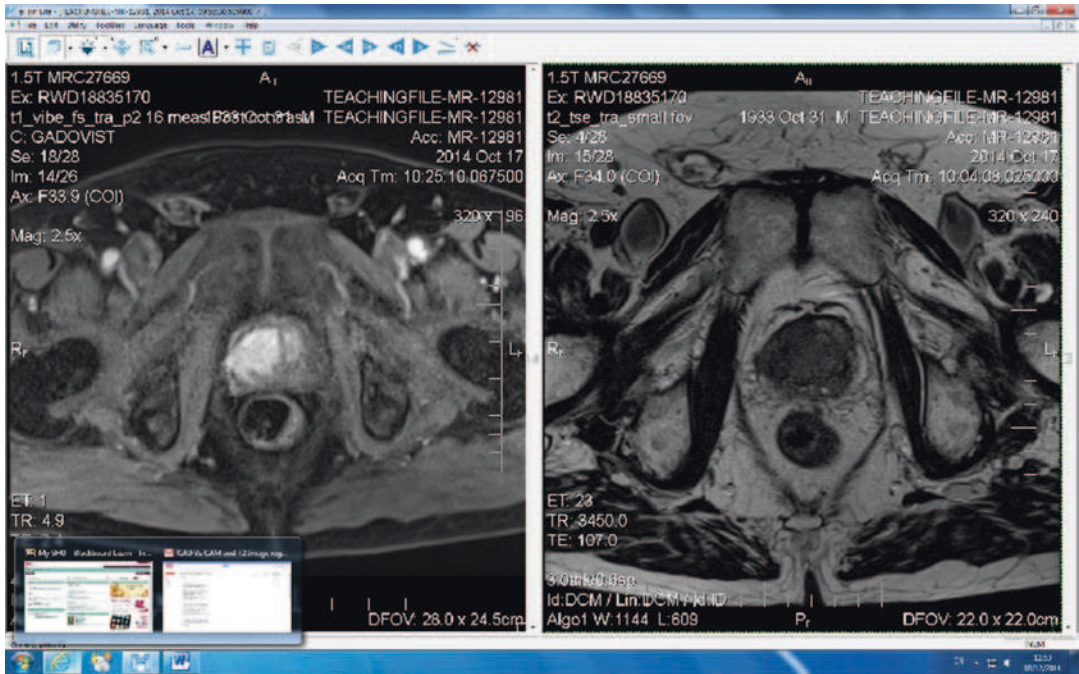


Fig. 24 Vendor provided DICOM viewer to display different image slices side by side. Using this facility it is easy to identify matching T2-weighted and the corresponding DCE MRI image of the same section



Fig. 25 T2-weighted MRI image section of the prostate with the prostate part of the image outlined. The HCS process will be applied within the boundary

- 2. Normally, diagnostic images are used by the radiologists to isolate boundaries around a tumor but in this case an attempt was made to visualize the details within a tumor. Also because of the lower resolution of the acquired MRI image data there were not enough pixels to resolve the finer details within the

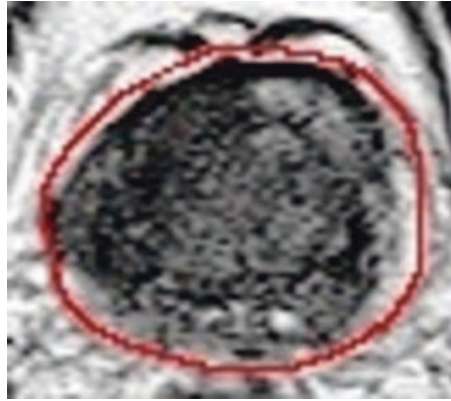


Fig. 26 The part of the T2-weighted MRI image which contains the prostate organ. The HCS process will be applied to this part of the image

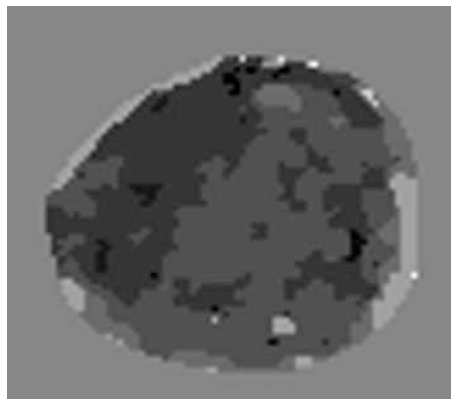


Fig. 27 Heat map image showing the different regions identified by the HCS process in processing T2-weighted MRI image. The different regions are shaded (*dark to bright*) based on the average pixel value of the region

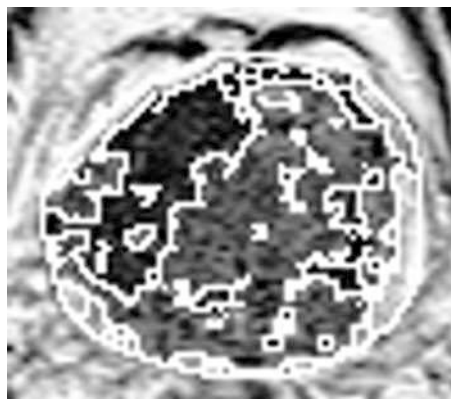


Fig. 28 The boundaries of the different regions identified by the HCS process in processing T2-weighted MRI image

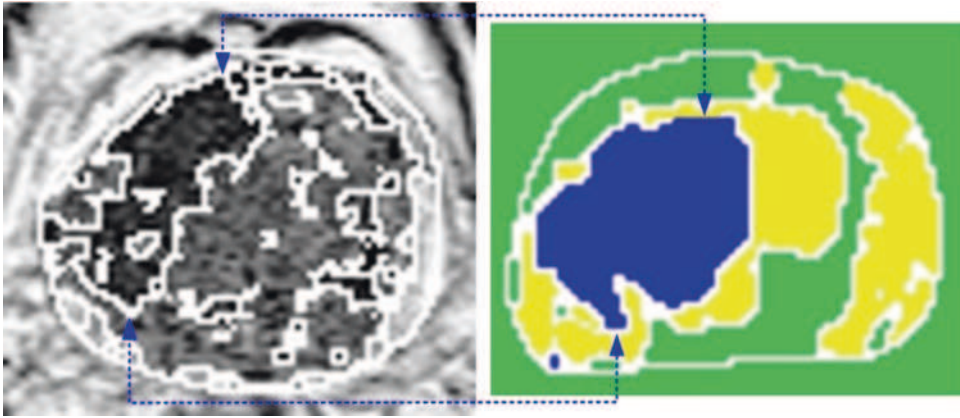


Fig. 29 Correlating HCS boundary outlined T2-weighted image (*left*) with the DCE-MRI TIC-based classified regions (*right*). The loss of signal in the T2-weighted image (*left*) matches with the DCE-MRI T2 region classified as carcinoma (*Blue region*), based on the six different types of enhancement patterns (Fig. 16)

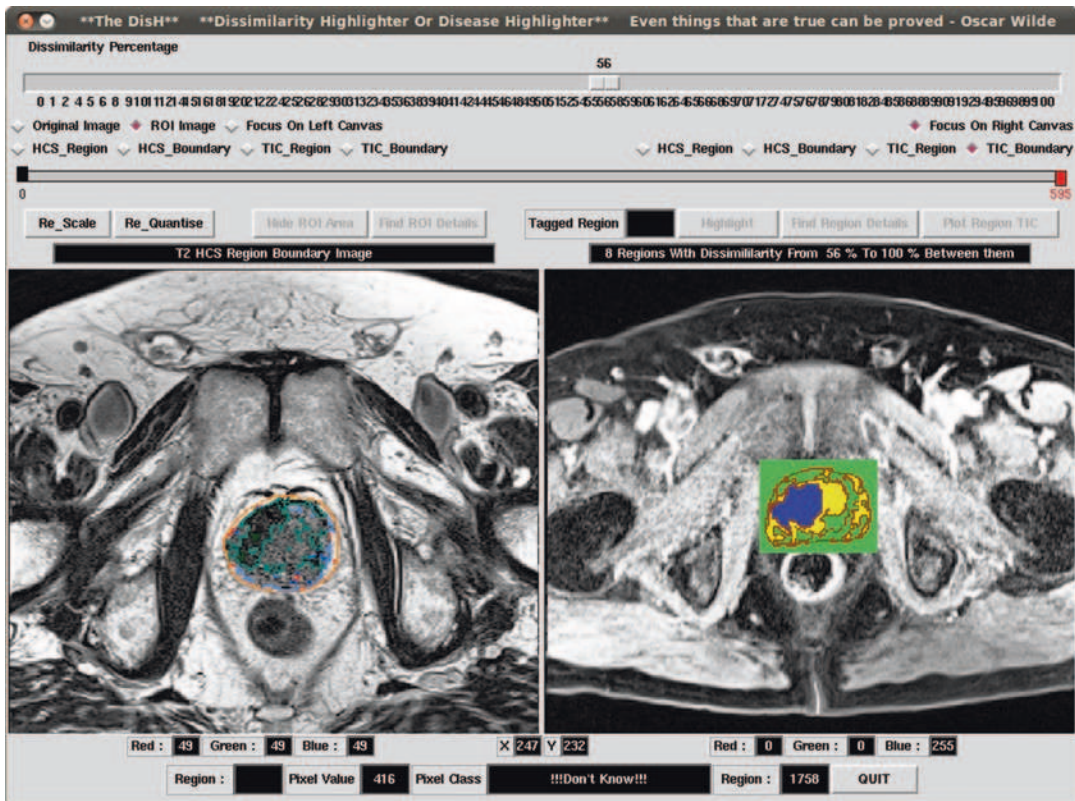


Fig. 30 Graphical User Interface (GUI) implemented as part of the study to view T2-weighted along with the DCE-MRI image slices to correlate the different regions identified by the HCS process

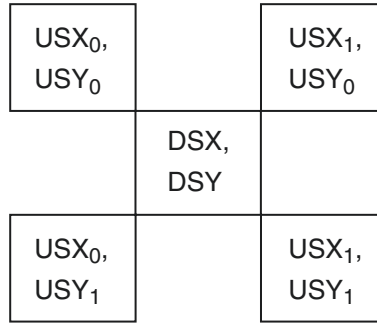


Fig. 31 The locations of the pixels in an image whose values will be used either to Up or Down sample the original image (For details see the text.)

tissue sample. To address this issue of sparsity of data in the original MR image, the original MR image data was Up-Sampled to twice its original size using Bi-Non-linear process (along both x and y directions). The Bi-Non-linear process is detailed below with an example.

Each of the pixels in the original image at the location (DSX, DSY) was replaced by four pixels in the Up-Sampled image at the locations (USX₀, USX₀), (USX₁, USY₀), (USX₀, USY₁), and (USX₁, USY₁) (Fig. 31).

The pixel values in the Up-Sampled image for the above four locations are estimated making use of the pixel values in the original image as follows:

$$\begin{aligned}
 [USX_0, USX_0] &= \{9 \times [DSX, DSY] + 3 \times [DSX, (DSY - 2)] + \\
 &3 \times [(DSX - 2), DSY] + [(DSX - 2), (DSY - 2)]\} \div 16 \\
 [USX_1, USX_0] &= \{9 \times [DSX, DSY] + 3 \times [DSX, (DSY - 2)] + \\
 &3 \times [(DSX + 2), DSY] + [(DSX + 2), (DSY - 2)]\} \div 16 \\
 [USX_0, USX_1] &= \{9 \times [DSX, DSY] + 3 \times [DSX, (DSY + 2)] + \\
 &3 \times [(DSX - 2), DSY] + [(DSX - 2), (DSY + 2)]\} \div 16 \\
 [USX_1, USX_1] &= \{9 \times [DSX, DSY] + 3 \times [DSX, (DSY + 2)] + \\
 &3 \times [(DSX + 2), DSY] + [(DSX + 2), (DSY + 2)]\} \div 16
 \end{aligned}$$

Figure 32 illustrates the performance of the implemented Bi-Non-Linear Up-Sampling process where a 256 × 256 original image was Up-Sampled to a 512 × 512 image.

3. The original FFDM X-ray mammogram data was of high resolution (70 μm pixel spacing). The HCS process is a processing intensive process (see Note 4). Hence to process the images in a reasonable time it was decided to down-sample the original image data to half its original resolution (along both x and y directions). For Down-Sampling the original image data Bi-Non-linear process as detailed below was adopted.

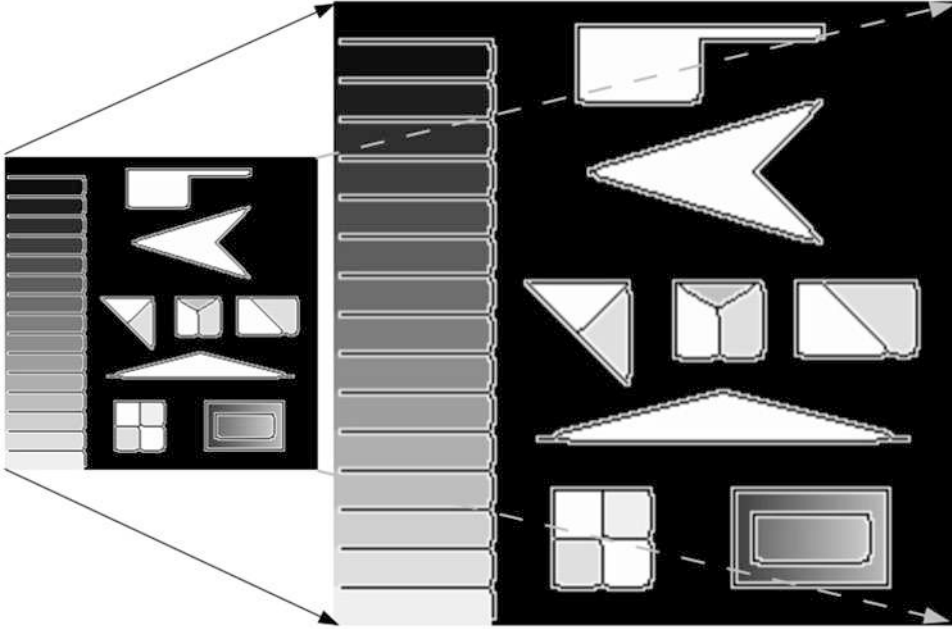


Fig. 32 Image illustrating the performance of the bilinear up-sampling algorithm

The four pixels in the original image at the locations (USX_0, USX_0) , (USX_1, USY_0) , (USX_0, USY_1) , and (USX_1, USY_1) were replaced with a pixel at the location (DSX, DSY) in the down-sampled image (Fig. 31).

The pixel value in the Down-Sampled image is estimated making use of the pixel values in the original image as follows:

$$\begin{aligned}
 [DSX, DSY] = & \{[(DSX - 1), (DSY - 1)] + 3 \times [DSX, (DSY - 1)] + 3 \times [(DSX + 1), (DSY - 1)] + \\
 & [(DSX + 2), (DSY - 1)] + 3 \times [(DSX - 1), DSY] + 9 \times [DSX, DSY] + \\
 & 9 \times [(DSX + 1), DSY] + 3 \times [(DSX + 2), DSY] + 3 \times [(DSX - 1), (DSY + 1)] + \\
 & 9 \times [DSX, (DSY + 1)] + 9 \times [(DSX + 1), (DSY + 1)] + \\
 & 3 \times [(DSX + 2), (DSY + 1)] + [(DSX - 1), (DSY + 2)] + \\
 & 3 \times [DSX, (DSY + 2)] + 3 \times [(DSX + 1), (DSY + 2)] + [(DSX + 2), (DSY + 2)]\} \div 64
 \end{aligned}$$

Figure 33 illustrates the performance of the implemented Bi-Non-Linear Down-Sampling process where a 512×512 original image was Down-Sampled to a 256×256 size image.

4. Other similar agglomerative hierarchical clustering or bottom-up methods suffer from the distorting phenomena, in which the cluster structures depend on order in which the regions are considered for merging [10]. But HCS process ensures that the segmentation of image into its constituent regions is always the same irrespective of the order in which image regions are processed [5]. This is achieved by the brute force approach, followed by the HCS process, where only those

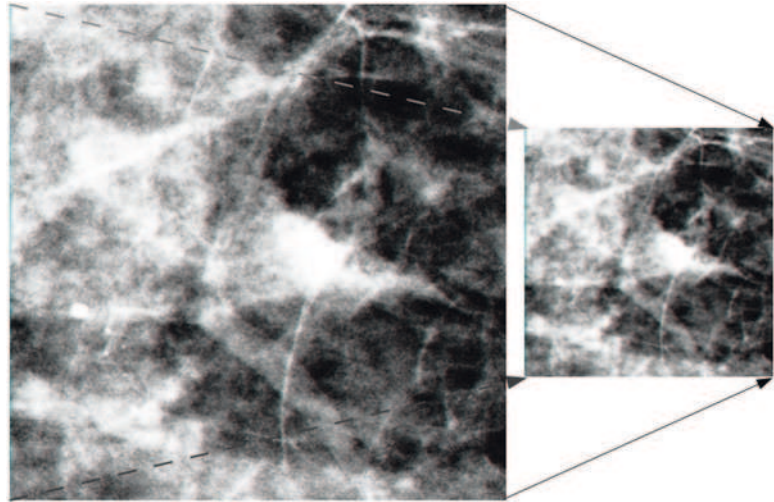


Fig. 33 Image illustrating the performance of the bilinear down-sampling algorithm

regions with the smallest overall dissimilarity are merged in each step, which is the only solution to overcome the distorting phenomena and achieve the same segmentation output consistently [16]. To accelerate the process of comparison of different regions in an image, the operation is done concurrently.

Border pixel reclassification is another unique feature of the HCS process (Fig. 7). Border pixel reclassification is considered only for those pixels on the boundary of the clusters which had been merged with other clusters. These boundary pixels are removed one at a time from their original clusters. The pixel removed is considered as a region of its own and the similarity between the one pixel region and the regions bordering it (which include the original cluster to which it belonged) is found and the single pixel region merged with the most similar bordering region. Border pixel reclassification aides in overriding local inhomogeneity while clustering similar pixels/regions. The positive effect of border pixel re-classification can be visualized in Fig. 34. It can be seen from the border outlined images the HCS process with border pixel reclassification (top row) achieves far better results in delineating the different regions of an ill-defined abnormality presented in a X-ray mammogram (middle row) when compared to the segmentation without border-pixel-re-classification (bottom row) (Fig. 34).

Because of the brute-force approach adopted by the HCS process, to ensure consistent segmentation and because of the border-pixel-re-classification operation which is a sequential operation the HCS process is a processing intensive process.

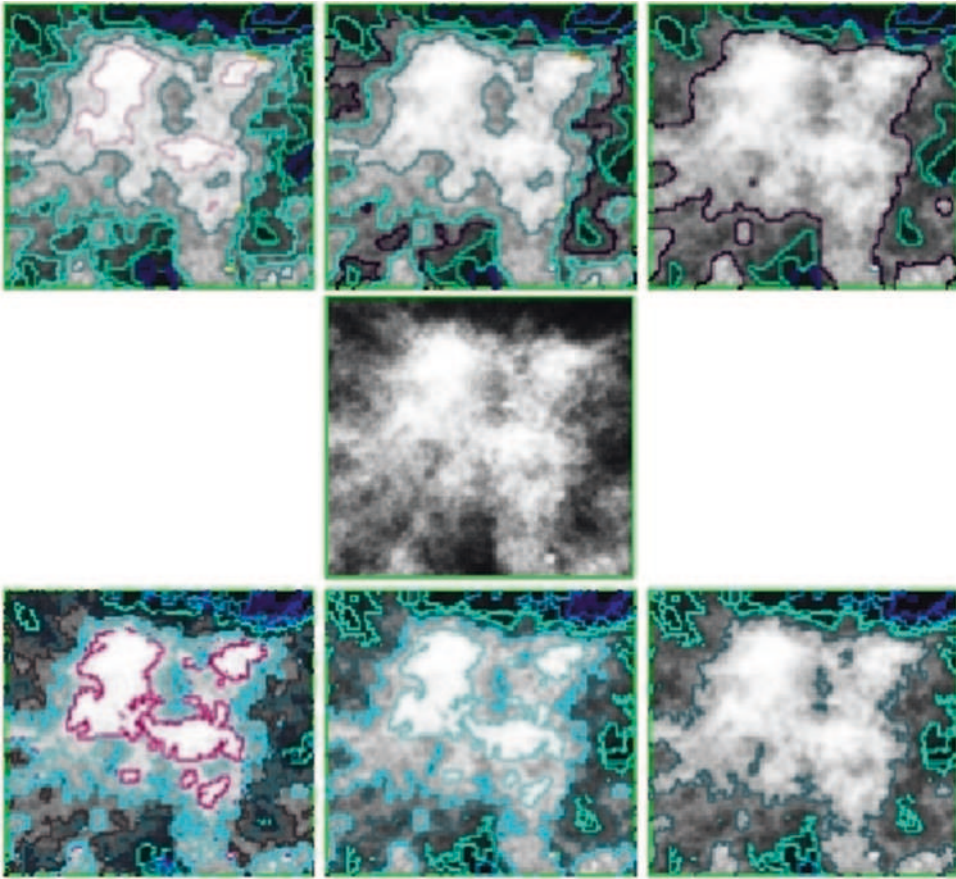


Fig. 34 An abnormality having ill-defined boundaries (*middle row*) processed by the HCS process with border pixel reclassification operation (*top row*) and without border pixel reclassification (*bottom row*). This is to illustrate how border pixel reclassification operation ensures more appropriate delineation of the ill-defined inner details of the abnormality

5. The feature measure used by the HCS process, to estimate the similarity between locations or regions within an image, is the actual distribution of the pixel values within a neighborhood surrounding the locations or within the regions. This technique may be considered to work in a way similar to the human visual system where features for texture (region) segmentation are not consciously computed [17].
6. The major limitation of the current study is that the acquired MRI image data was of low spatial resolution of only $500\ \mu\text{m}$ (*see Notes 1 and 2*), while the MALDI-MSI image was acquired using raster/spot to spot imaging mode at $100\ \mu\text{m}$ spatial resolution. However, still, HCS process segmented abnormal regions correlated with the MALDI-MSI. Hence, one can only expect improvements in the current results if

image data from higher field strength device, capable of higher resolutions like $100\ \mu\text{m}$, is used.

7. Even though the original FFDM data was down-sampled before processing, the finer details of the image was still preserved. This is because to start with the original image data was of high resolution ($70\ \mu\text{m}$) and subsampling resulted in an image of $140\ \mu\text{m}$ pixels spacing that is still of high resolution.

Since the HCS process is robust enough to handle image data of very low resolution ($250\ \mu\text{m}$), the processing of the down-sampled image data ($140\ \mu\text{m}$) still facilitated visualization of finer details within the abnormality (Fig. 12).

8. To interpret the DCE-MRI data, by making use of TIC characteristics, machine vendors provide the radiologists with the facility to select a region of interest (ROI) enclosing an area of the largest enhancement and subsequently observe how the average signal intensity of the voxels within the ROI varies with time (Fig. 35).

The ROI, normally chosen within an area of the largest enhancement, because of tissue heterogeneity, may enclose tissues of different enhancement patterns (Green boundary Fig. 36a). Hence, the averaged TIC from the ROI may not represent the actual characteristics of the lesion.

To overcome the approximation, intrinsic to the TIC estimated on pixels averaged within the radiologist drawn ROI, recent studies have proposed to estimate and classify the TIC in every single voxel acquired by the DCE-MRI scan sequence [18].

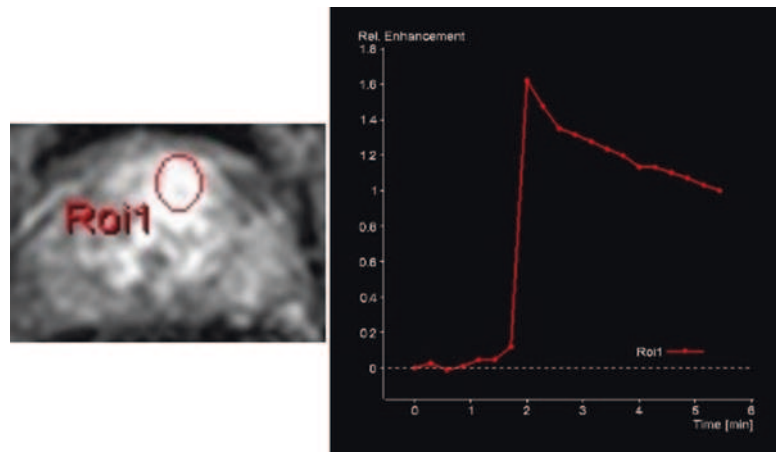


Fig. 35 Region of interest (ROI) selected by the radiologist, enclosing an area of the largest enhancement and the corresponding enhancement pattern, of the locations within the ROI, with time (TIC). (This facility is provided by the MRI machine vendor)

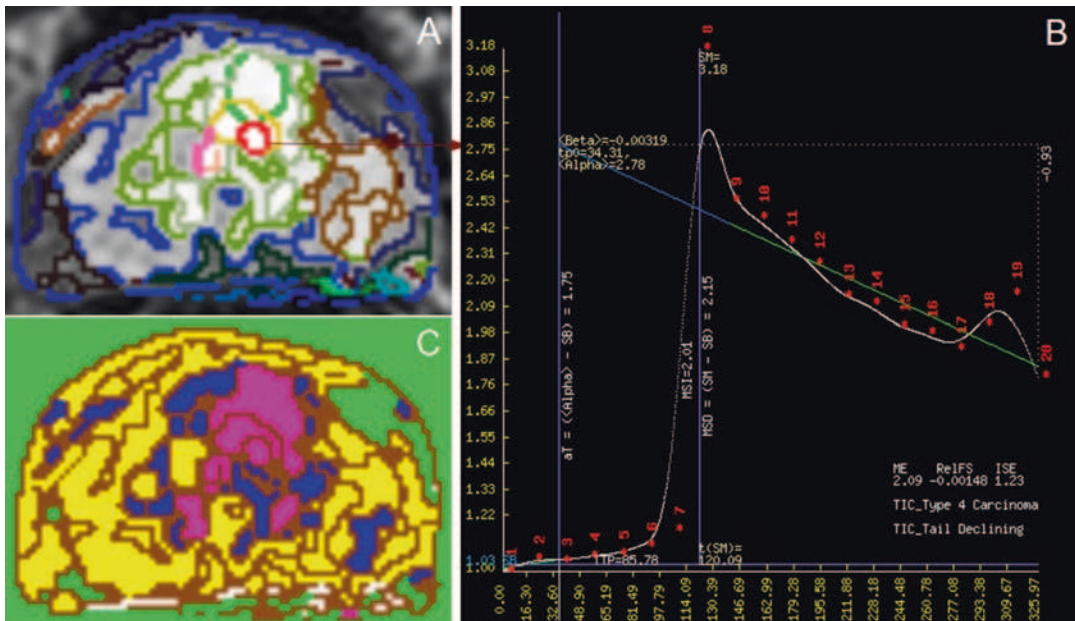


Fig. 36 ROI selected by the radiologist, enclosing tissues of different enhancement patterns (Green boundary) (a). Making use of the HCS process segmented regions user objectively chooses a more appropriate ROI (Red boundary) (a). Parametric illustration of the TIC for the user chosen ROI (b). Automated color-coded classification, of the HCS process’ different regions, based on the TIC enhancement pattern of the regions (c). (The color coding is based on the six different types of enhancement patterns (Fig. 16))

The limitations of the pixel by pixel analysis of the TIC are as follows:

- Pixel-by-pixel analysis of the TIC is sensitive to pixels having different enhancement patterns [19].
- Pixel-by-pixel analysis of the TIC excludes the user from the diagnostic process.
- The resulting classification does not provide any indication regarding how and why pixels are classified as belonging to a specific type which might lead to the situation where incorrect CAD can have a detrimental effect on human decisions [20, 21].

The demonstrated HCS process-based TIC classifier method offers the benefits of both the ROI and pixel-by-pixel analysis approaches. The HCS process segmented regions enable the user to objectively choose a more appropriate ROI (Red boundary Fig. 36a) and to view a more representative parametric illustration of the TIC (Fig. 36b).

Also, the HCS process-based method presents the user with the automated color-coded classification of the different regions based on the TIC enhancement pattern of the HCS process’s regions (Fig. 36c). The color coding is based on the six different types of enhancement patterns (Fig. 16).

References

1. Chandarana H, Rosenkrantz AB, Mussi TC, Kim S, Ahmad AA, Raj SD, McMenemy J, Melamed J, Babb JS, Kiefer B, Kiraly AP (2012) Histogram analysis of whole-lesion enhancement in differentiating clear cell from papillary subtype of renal cell cancer. *Radiology* 265:790–798
2. Fitzpatrick JM, Sonka M (eds) (2000) *Handbook of medical imaging volume 2 medical image processing and analysis*. SPIE-the international society for optical engineering. ISBN-10: 0819477605
3. Arbelaez P (2006) Boundary extraction in natural images using Ultrametric contour maps. *Proceedings 5th IEEE workshop on perceptual Organization in Computer Vision (POCV'06)*, New York, June 2006 (paper presented at a conference)
4. Arbelaez P, Fowlkes C, Martin D (2007) The Berkeley segmentation dataset and benchmark. <http://www.Eecs.Berkeley.Edu/research/projects/CS/vision/bsds/>. Accessed 27 Jun 2016
5. Selvan AN (2007) Highlighting dissimilarity in medical images using hierarchical clustering-based segmentation (HCS). M.Phil. Dissertation, Faculty of Arts Computing Engineering and Sciences, Sheffield Hallam University, Sheffield, UK
6. Selvan AN (2011) Boundary extraction in images using hierarchical clustering-based segmentation (HCS). Paper presented at the British machine vision conference (student workshop), Dundee, UK, Sept 2011
7. Selvan AN (2012) Hierarchical clustering-based segmentation (HCS) aided diagnostic image interpretation and monitoring. Doctoral dissertation, Faculty of Arts Computing Engineering and Sciences, Sheffield Hallam University, Sheffield, UK
8. Cole LM, Selvan AN, Wright C, Reed H, Clench MR (2014) Communication of medical images to diverse audiences using multiple imaging modalities. Poster presented in British mass spectrometry society, Cheshire, UK, 1–2 April 2014
9. Ohlander R, Price K, Reddy R (1978) Picture segmentation by a recursive region splitting method. *Comput Graph Image Process* 8:313–333
10. Nadler M, Smith EP (1993) *Pattern recognition engineering*. John Wiley and Sons, New York
11. Cole LM, Selvan AN, Partridge R, Reed H, Wright C, Clench MR (2015) Communication of medical images to diverse audiences using multimodal imaging. *Adv Struct Chem Imag* 1:13
12. Naylor S, Spackman L and Selvan AN (2015) Evaluation of hierarchical clustering-based segmentation as a perception aid for mammogram readers. Poster presented in UK radiological congress, ACC, Liverpool, UK, 29 June–1 July 2015
13. Vos CP, Hambrock T, Barenstz JO, Huisman HJ (2010) Computer-assisted analysis of peripheral zone prostate lesions using T2-weighted and dynamic contrast enhanced T1-weighted MRI. *Phys Med Biol* 55(6):1719–1734
14. Engelbrecht MR, Huisman HJ, Laheij RJ et al (2003) Discrimination of prostate cancer from normal peripheral zone and central land tissue by using dynamic contrast-enhanced MR imaging. *Radiology* 229:248–254
15. Lavini C, de Jonge MC, van de Sande MG, Tak PP, Nederveen AJ, Maas M Pixel-by-pixel analysis of DCE MRI curve patterns and an illustration of its application to the imaging of the musculoskeletal system. *Magn Reson Imaging* 25(5):604–612
16. Thies C, Malik A, Keyzers D, Kohnen M, Fischer B, Lehmann TM (2003) Content-based retrieval in medical image databases by hierarchical feature clustering. *Proc SPIE* 5032:598–608
17. Bhattacharya U, Chaudhuri BB, Parui SK (1997) An MLP-based texture segmentation method without selecting a feature set *Image and Vis Comput* 15 937–948
18. Lavini C et al (2007) Pixel-by-pixel analysis of DCE MRI curve patterns and an illustration of its application to the imaging of the musculoskeletal system. *MRI* 25(5):604–612
19. Lavini C, Buitter SM, Maas M (2013) Use of dynamic contrast enhanced time intensity curve shape analysis in MRI: theory and practice. *Rep Med Imag* 2013:71–82
20. Alberdi E et al (2005) Use of computer-aided detection (CAD) tools in screening mammography: a multidisciplinary investigation. *Br J Radiol* 78:31–40
21. Fenton JJ et al (2011) Effectiveness of computer-aided detection in community mammography practice. *J Natl Cancer Inst* 103(15):1152–1161